

Graph Reinforcement Learning for Predictive Power Allocation to Mobile Users

Jianyu Zhao and Chenyang Yang

Abstract

Allocating resources with future channels can save resource to ensure quality-of-service of video streaming. In this paper, we optimize predictive power allocation to minimize the energy consumed at distributed units (DUs) by using deep deterministic policy gradient (DDPG) to find optimal policy and predict average channel gains. To improve training efficiency, we resort to graph DDPG for exploiting two kinds of relational priors: (a) permutation equivariant (PE) and permutation invariant (PI) properties of policy function and action-value function, (b) topology relation among users and DUs. To design graph DDPG framework more systematically in harnessing the priors, we first demonstrate how to transform matrix-based DDPG into graph-based DDPG. Then, we respectively design the actor and critic networks to satisfy the permutation properties when graph neural networks are used in embedding and end-to-end manners. To avoid destroying the PE/PI properties of the actor and critic networks, we conceive a batch normalization method. Finally, we show the impact of leveraging each prior. Simulation results show that the learned predictive policy performs close to the optimal solution with perfect future information, and the graph DDPG algorithms converge much faster than existing DDPG algorithms.

Index Terms

Reinforcement learning, graph neural network, predictive power allocation, training complexity

I. INTRODUCTION

Deep reinforcement learning (DRL) has been widely applied for resource allocation [1], thanks to the ability of making decision for complicated tasks without mathematical model, training online without labels hence capable of adaptive to dynamic environments, and finding good policies from non-convex or NP-hard problems with low inference complexity [2–9].

One of model-free applications is predictive resource allocation (PRA) [10–14]. Different from existing non-predictive approaches, PRA optimizes future radio resources with the channel conditions to be experienced by mobile users, which can leverage past observations for channels. With the predicted average channel gains or average data rates in a minute-level horizon, PRA has

been shown able to save energy or improve throughput remarkably with respect to non-predictive counterpart for video streaming [15–19], which accounts for majority of global mobile data [20].

However, DRL still faces limitations in training efficiency. In particular, DRL is with high sample complexity and poor generalizability [21]. The training procedure for a DRL model is lengthy and costly. Before convergence, the decision made by the DRL incurs poor performance. For mobile users that may travel across multiple cells during video streaming, a centralized unit (CU) connected with multiple distributed units (DUs) need to train a learning model by interacting with environment continuously, where the CU and DUs exchange data in each time step. With high sample complexity, too many episodes are required for converging to a desirable performance, and large signaling overhead incurs since each episode contains many time steps. On the other hand, since wireless networks are usually non-stationary, it is hard for a converged DRL model operates with acceptable performance in an unseen environments.

To handle these challenges, an effective approach is to exploit prior knowledge for designing the structure of deep neural networks (DNNs). One kind of relational prior, permutation equivalence (PE) and permutation invariance (PI) properties of multivariate functions [22], has been noticed widely-existed in wireless resource allocation policies [23, 24]. By introducing parameter sharing into fully-connected neural networks (FNNs), permutation equivalence neural network (PENN) or permutation invariance neural network (PINN) can incorporate the permutational priors into the DNN structure [22]. Another relational prior naturally existed in wireless networks is the topology relation among nodes (say CU and DUs), which can be characterized explicitly by graph. By learning over graph, graph neural networks (GNNs) are possible to harness both kinds of relational priors for improving training efficiency.

A. Related Works

1) Predictive resource allocation: Early works of PRA for video streaming optimize resource allocation policies assuming that perfect future information in a prediction window is known [15, 18, 19] or optimize robust policies by further assuming that the statistics of prediction errors are known [17]. Encouraged by the success of machine learning, recent works first make the prediction with off-line trained learning model and then optimize the policy with the predicted information [11, 16]. By resorting to DRL algorithms, the information prediction and policy optimization can be accomplished online in a single step towards the same objective. As illustrated in [4], the DRL solution of an energy-saving PRA policy for a single mobile

user is superior to the first-predict-then-optimize solution, which however is with high sample complexity due to not exploiting prior knowledge.

2) *GNN for resource allocation*: GNNs have been employed to optimize power allocation and link scheduling with deep learning [24–27], and shown with good scalability, generalizability, and low training complexity by harnessing relation priors. GNNs have also been introduced to DRL for wireless resource allocation recently, where the state is represented by graph instead of matrix or vector in FNN-based DRL [28–30]. To improve learning performance by extracting information from graph, a GNN was used to approximate Q-function to learn a channel allocation policy in [28]. To develop a scalable policy, GNN was integrated with deep Q-network to optimize user association in [29]. To improve generalization ability in different network topologies, GNN was incorporated into REINFORCH to optimize network function virtualization placement in [30]. Compared with deep learning where DNNs are trained offline, reducing sample complexity of DRL is more important, which however has not been addressed for GNN-based DRL.

B. Motivation and Contributions

Although GNNs are able to harness both topological prior and permutational prior, it is challenging to fully unleash the power of GNNs in leveraging the priors. This is because GNNs are highly flexible with diverse choices for graph, combiner and aggregator, *etc.*, and GNNs can be used in two manners [31]. One is the embedding manner that using a GNN to represent vertexes as vector representations, and then using output layers (say fully-connected layers) to obtain the policy of a task [26, 28, 29]. Another is the end-to-end manner that directly employing GNNs to obtain the policy [25, 27].

The topological prior can be exploited by message passing over a well-designed graph. Hence, appropriately formulating a graph is critical for GNN to perform well, which however needs trial-and-error process because graph is not unique for a problem [27]. On the other hand, designing state in DRL framework for a specific problem is tricky, and trial-and-error process is also inevitable. Unfortunately, there is no general method to design the problem-dependent state. The graphs in existing graph DRL frameworks [28–30] are designed directly from the considered problems. Yet DRL frameworks have been established with judiciously designed states for a variety of resource allocation problems [2–9], where the state and action are represented by matrices or vectors. Then, a natural question is: can we translate a matrix-based DRL framework into a graph-based DRL framework?

To exploit the second prior, GNNs need to be carefully designed. While GNNs naturally exhibit some sorts of PE or PI properties, they may not match with the properties of a policy. This incurs learning performance degradation of a GNN [27]. To satisfy the permutational properties of a policy, GNNs can be designed from three aspects. The first is the parameter sharing scheme, which decides the properties of the parameterized function family represented by a GNN when a graph has been designed. The second is the output layer when GNNs are used in the embedding manner, since properties of the output layer affect the properties of the whole neural network. The third is batch normalization. Vanilla batch normalization proposed in [32] normalizes each scalar feature in a sample by estimating the mean and variance of features. However, the values of mean and variance will be changed when the order of features in some samples in a batch is changed, which may destroy the permutational properties of the DNN.

While generalizability is also important, in this paper, we strive to design graph DRL framework for reducing sample complexity by exploiting relational priors more systematically. To this end, we consider a typical model-free task that should employ DRL and is with complicated permutational properties, which is to optimize predictive power allocation among mobile users to minimize the average transmit power consumed at the DUs for video streaming with quality-of-service (QoS) constraint of each user. Since the action lies in continuous space, we consider deep deterministic policy gradient (DDPG) algorithm.

The major contributions are summarized as follows.

- We showcase how to transform the matrix-based DRL framework into graph-based DRL framework, by extending the DDPG framework for predictive power allocation among future frames in prediction window of a single user in [4] to multiple users. This facilitates to harness the topological prior with GNN by reusing the already-designed states in literature, and shows the difference between GNN and PENN as a by-product.
- We design the GNNs to satisfy the combinational PE and PI properties of the policy function and action-value function in DDPG to optimize predictive power allocation. We introduce a generic method to construct parameter sharing schemes for GNNs, design the output layers for the embedding manner, and conceive a batch normalization method for reserving the permutational properties, which are also applicable to deep learning.
- We analyze the impacts of harnessing the two kinds of relational priors in DRL algorithms on the learning performance, training complexity and the signaling overhead before convergence, and compare the performance of using GNNs in the two manners. Simulations show

that the proposed DDPG algorithms need much lower training complexity and signaling overhead than the FNN-based DDPG algorithm to achieve the same learning performance.

II. SYSTEM MODEL AND PROBLEM FORMULATION

Consider a system where M DUs connected with a CU serve K mobile users requesting video streaming. The CU records the status of each user via the DUs, learns a resource allocation policy for the users, and controls the DUs to execute the policy by sending instructions.

Each video is divided into N_v segments. The playback duration of each segment is divided into N_f time frames, each with duration ΔT . Each frame contains N_s time slots, each with duration τ . The durations of each frame and each time slot are defined according to the coherence time of large-scale and small-scale channel gains, respectively.

For video streaming, if each segment can be downloaded to the buffer of a user before playback, no stalling occurs, and then the QoS of the user will be satisfied.

After a user initiates a request for a video, the first segment (denoted as the $(n_v = 0)$ th segment) of the video has to be delivered in a non-prediction manner, during which the channels of the user can be gathered to facilitate channel prediction for subsequent $N_v - 1$ segments. If the future channels are perfect, then the transmit powers allocated among users in future time slots of the $(N_v - 1)N_f$ frames can be optimized to minimize the average total transmission energy at the DUs required to ensure the QoS of every user during video streaming as follows,

$$\min_{\{p_{tj}^k\}} \mathbb{E} \left[\sum_{k=1}^K \left(\sum_{t=1}^{(N_v-1)N_f} \left(\sum_{j=1}^{N_s} \tau p_{tj}^k \right) \right) \right] \quad (1a)$$

$$s.t. \sum_{n=1}^{n_v} \sum_{t=(n-1)N_f+1}^{nN_f} \sum_{j=1}^{N_s} \tau R_{tj}^k \geq \sum_{n=2}^{l+1} d_n^k, \quad n_v = 1, \dots, N_v - 1, k = 1, \dots, K, \quad (1b)$$

where the average in (1a) is taken over both large-scale and small-scale channel gains, (1b) is the QoS constraint of every user, p_{tj}^k and R_{tj}^k are respectively the instantaneous transmit power allocated to and the data rate achieved by the k th user in the j th time slot of the t th frame, and d_n^k is the number of bits of the n th segment in the video requested by the k th user.

In practice, future large-scale and small-scale channel gains are unknown, and prediction is never perfect. Instead of solving the problem with traditional optimization tools by treating the predicted channel as real channel, one can resort to DRL, which is powerful in dealing with model-free problems and is able to make optimization with implicitly predicted channels.

Considering that the problem can be naturally formulated as a Markov decision process with continuous optimization variables, the FNN-based DDPG algorithm proposed in [33] was employed to optimize the powers allocated to future frames for a single user in [4], where the inputs of FNNs are expressed as vectors. For the multi-user scenario in problem (1), relational priors can be exploited by designing GNN-based DDPG framework.

III. GRAPH DRL FRAMEWORK FOR PREDICTIVE POWER ALLOCATION

We call the DRL using matrix or vector to represent the input of neural networks as matrix-based DRL framework, since vectors are special matrices. In this section, we first extend the matrix-based DDPG framework for predictive power allocation to a single user in [4] into multiple users. Then, we show how to transform the matrix-based DDPG into graph-based DDPG framework, where the inputs of neural networks are graphs.

A. Matrix-based DRL Framework for Multiple Users

1) *Action*: By using similar analysis as in [4], it is not hard to show that the problem in (1) can be solved equivalently by first optimizing the average rates for all future frames, $\bar{R}_t^k \triangleq \mathbb{E}_g[R_{tj}^k], t = 1, \dots, (N_v - 1)N_f$, and then using \bar{R}_t^k to obtain $p_{tj}^k, j = 1, \dots, N_s$. To reduce the signaling overhead between the CU and DUs, we set \bar{R}_t^k instead of p_{tj}^k as the action for the k th user. Then, the duration of a time step in the DRL formulation is equal to the frame duration. The action vector of all users in the t th time step can be expressed as,

$$\mathbf{a}_t = [\bar{R}_t^1, \dots, \bar{R}_t^K]^\top, \quad (2)$$

where $[\cdot]^\top$ denotes transpose.

2) *State*: According to [4], the state of the k th user at time step t is composed of B_t^k, f_t^k, η_t^k , and $\boldsymbol{\alpha}_{t-T}^k, \dots, \boldsymbol{\alpha}_t^k$, where T is a pre-determined value affecting the performance of the implicit channel prediction. B_t^k is the amount of data in the buffer of the k th user at time step t , $f_t^k \in [0, \dots, N_v - 1]$ is the frame index of the video segment the k th user playback at time step t , η_t^k is the ratio of amount of data having been delivered to the k th user at time step t to the total amount of data in the video requested by the user. $\boldsymbol{\alpha}_t^k \triangleq [\alpha_{t,1}^k, \dots, \alpha_{t,N_b}^k]^\top$, $\alpha_{t,i}^k$ is the large-scale channel gain from the i th neighbouring DU to the k th user at time step t , $i = 2, \dots, N_b$, and $\alpha_{t,1}^k$ is the large-scale channel gain between the k th user and its associated DU.

For the multi-user scenario, a DU may serve multiple users in a time step. To help the agent learn the power allocation policy among the users that are associated with the same DU, the index of the DU that the k th user is associated with at time step t , denoted as M_t^k , needs to be included in the state. Then, the state vector of the k th user can be expressed as

$$\mathbf{s}_t^k \triangleq [B_t^k, f_t^k, \eta_t^k, M_t^k, \boldsymbol{\alpha}_{t-T}^{k\top}, \dots, \boldsymbol{\alpha}_t^{k\top}]^\top, \quad (3)$$

where $\boldsymbol{\alpha}_t^{k\top}$ is the transpose of $\boldsymbol{\alpha}_t^k$ (i.e., $(\boldsymbol{\alpha}_t^k)^\top$). The state matrix is $\mathbf{S}_t = [\mathbf{s}_t^1, \dots, \mathbf{s}_t^K]^\top$.

3) *Reward*: If the constraints in (1b) are not satisfied by the learned action \mathbf{a}_t at time step $t = lN_f$, $l = 1, \dots, N_v - 1$, one can employ the safe layer method [34] where action \mathbf{a}_t is projected into $\tilde{\mathbf{a}}_t$ by solving the following optimization problem,

$$\min_{\tilde{\mathbf{a}}_t} \|\mathbf{a}_t - \tilde{\mathbf{a}}_t\|_2 \quad (4a)$$

$$s.t. \mathbf{a}_1 + \dots + \mathbf{a}_{t-1} + \tilde{\mathbf{a}}_t \geq \sum_{n=2}^{l+1} \mathbf{d}_n, \quad (4b)$$

where $\mathbf{d}_n \triangleq [d_n^1, \dots, d_n^K]^\top$, composing the numbers of bits of the n th segment in the videos requested by all users. At time step t , both $\sum_{n=2}^{l+1} \mathbf{d}_n$ and $\sum_{i=1}^{t-1} \mathbf{a}_i$ are known. Thereby the solution of the problem can be obtained as

$$\tilde{\mathbf{a}}_t = \sum_{n=2}^{l+1} \mathbf{d}_n - \sum_{i=1}^{t-1} \mathbf{a}_i, \quad (5)$$

which can be used to adjust the learned action for satisfying the constraint.

Then, the reward for the agent can be set as the negative value of the total energy consumed at BSs by delivering the videos requested by the users at time step t , i.e.,

$$r_t = - \sum_{k=1}^K \sum_{j=1}^{N_s} \tau p_{tj}^k. \quad (6)$$

In each time slot of time step t , the BS that serves the k th user can compute p_{tj}^k , $j = 1, \dots, N_s$ from \mathbf{a}_t or $\tilde{\mathbf{a}}_t$ with the method in [4] and transmit to the user. Then, the BS computes $\sum_{j=1}^{N_s} \tau p_{tj}^k$ and uploads to the CU to calculate r_t in time step t .

B. Graph-based DRL Framework for Multiple Users

DDPG algorithm maintains an actor network to learn the policy function that maps the *state* into the action, and a critic network to learn the action-value function that maps the *state-action* into the expected return. The state and state-action pair can be represented with graphs, which consist of vertexes, edges and their features. In the following, we show how to transform the matrix-based DDPG in section III-A into graph-based DDPG framework, i.e., to formulate the *state graph* and *state-action graph* from the state matrix in (3) and action vector in (2).

1) *Obtain vertexes and edges*: Before defining the vertex set and edge set, we first need to determine if the state graph and state-action graph are with fixed or dynamic topology. If the graphs are topology fixed, then all nodes in the system (i.e., DUs and users) relevant to the state and action over all time steps can be set as vertexes, and the relationships among the vertexes over all time steps can be set as edges. Then, the vertex and edge sets are constant over time, while their features may be time-varying. If the graphs are topology dynamic, we only find the nodes and relationships involved in state and action at time step t , and set them respectively as vertexes and edges. Then, both the vertex and edge sets as well as their features change over time. For easy exposition, we consider topology fixed graphs as an illustration.

The state and action in section III-A involve two types of nodes, users and DUs. We define each user or each DU as a vertex. Denote the sets of user vertexes or DU vertexes as \mathcal{U} or \mathcal{B} . For mobile users, since a user may be served by different DUs at different time steps during video streaming, there is an edge between every user and every BS. There are no edges between DUs or between users, because a DU does not communicate with other DUs and a user does not communicate with other users in the considered system. Denote the set of edges as \mathcal{E} .

\mathcal{U} , \mathcal{B} and \mathcal{E} are the same for the state graph and the state-action graph.

2) *Obtain features*: In the *state graph*, the features of vertexes and edges can be obtained from the state matrix. If an element in state matrix involves only one vertex, the element can be set as a feature of the vertex. If an element involves two vertexes, then the element can be transformed into a feature of the edge connecting the two vertexes.

The state vector for the k th user \mathbf{s}_t^k in (3) can be divided into two terms as $[B_t^k, f_t^k, \eta_t^k]^\top$ and $[M_t^k, \boldsymbol{\alpha}_{t-T}^{k\top}, \dots, \boldsymbol{\alpha}_t^{k\top}]^\top$.

Since the first term only involves the vertex representing the k th user, we set $[B_t^k, f_t^k, \eta_t^k]^\top \triangleq \mathbf{u}_t^k$ as the feature of the k th user vertex in state graph at time step t . Then, the feature matrix of all user vertexes in the state graph at time step t is $\mathbf{U}_t = [\mathbf{u}_t^1, \dots, \mathbf{u}_t^K]^\top$.

The second term involves DU vertexes and user vertexes, which can be transformed into the features of edges. Recall that M_t^k is the index of the DU that the k th user is associated with at time step t , which only reflects the relationship between the k th user and its associated DU but cannot reflect its relationship with the unassociated DUs. Since there is an edge between the k th user and every DU, we introduce an association indicator $I_t(m, k)$ into the feature of the edges, where $I_t(m, k) = 1$ if the k th user is associated with the m th DU at time step t , and $I_t(m, k) = 0$ otherwise. Further considering that when the k th user is not associated with the m th DU

at time step t , the large-scale channel gain between them is not useful for power allocation to the user, we set $\alpha_{t,m}^k I_t(m, k)$ as a feature of the edge connecting the k th user vertex and the m th DU vertex at the time step. Then, if the k th user is associated with the m th DU at time step t , $\alpha_{t,m}^k I_t(m, k) = \alpha_{t,m}^k$, and $\alpha_{t,m}^k I_t(m, k) = 0$ otherwise. The feature matrix of all edges in the state graph at time step t can be expressed as \mathbf{E}_t , whose element in the k th row and m th column is the feature vector of the edge between the k th user vertex and the m th DU vertex at time step t , which can be expressed as

$$\mathbf{e}_{t,m}^k = [\alpha_{t-T,m}^k I_{t-T}(m, k), \dots, \alpha_{t,m}^k I_t(m, k)]^\top. \quad (7)$$

In the *state-action graph*, the action (i.e., the average rates of all users) can be seen as a feature of user vertexes. Therefore, the feature vector of the k th user is $\tilde{\mathbf{u}}_t^k \triangleq [B_t^k, f_t^k, \eta_t^k, \bar{R}_t^k]^\top$, and the feature matrix of all user vertexes in the graph at time step t is $\tilde{\mathbf{U}}_t = [\tilde{\mathbf{u}}_t^1, \dots, \tilde{\mathbf{u}}_t^K]^\top$. The feature matrix of all edges in the state-action graph at time step t is also \mathbf{E}_t .

3) *Check whether each vertex is distinguishable*: If different vertexes can not be differentiated, the second kind of relational prior information will lose during training, which may lead to the increase of training complexity. The vertexes in a graph can be distinguished either by their features or by the features of the edges between them.

For the state and state-action graphs of the considered problem, if a DU is not associated with any users from the $(t - T)$ th time step to the t th time step, then the features of all the edges connected with the DU vertex are $[0, \dots, 0]^\top$, as shown in (7). If each DU vertex is not defined with feature, then the DU vertexes not associated with users within $(T + 1)$ time steps can not be distinguished and hence will be regarded as one vertex by the agent. As a result, the state and state-action graphs degenerate into another two graphs with lower dimensional adjacent matrixes. Take the state graph as an example, as illustrated in Fig. 1, the left graph degenerates into the right graph if the two DU vertexes in the ellipse can not be distinguished, and partial relation information (i.e., the red elements in the adjacent matrix on the left) will lose.

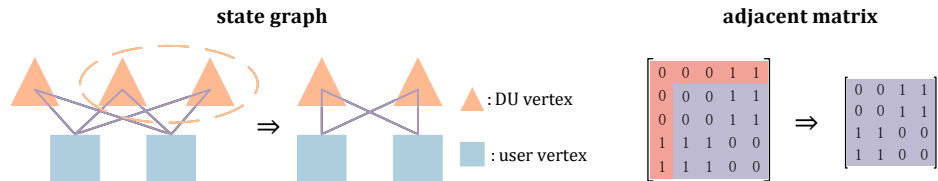


Fig. 1. Degeneration of state graph and adjacent matrix. The element in the i th row and the j th column of an adjacent matrix is 1 if there is an edge between the i th vertex and the j th vertex of a graph, and 0 otherwise.

Therefore, one should check if all the vertexes without features can be distinguished by the features of edges connecting them. If not, these vertexes should be defined with features. For the considered state and state-action graphs, we set the feature of the m th DU as $b_t^m \triangleq m$. Then, the feature vector of all DU vertexes at time step t is $\mathbf{b}_t = [b_t^1, \dots, b_t^M]^\top$.

Finally, the **state graph** and **state-action graph** can be respectively expressed as

$$S_t^G = \{ \underbrace{\{\mathcal{U}, \mathcal{B}\}}_{\text{vertexes}}, \underbrace{\mathcal{E}}_{\text{edges}}, \underbrace{\{\mathbf{U}_t, \mathbf{b}_t, \mathbf{E}_t\}}_{\text{features}} \}, \quad SA_t^G = \{ \underbrace{\{\mathcal{U}, \mathcal{B}\}}_{\text{vertexes}}, \underbrace{\mathcal{E}}_{\text{edges}}, \underbrace{\{\tilde{\mathbf{U}}_t, \mathbf{b}_t, \mathbf{E}_t\}}_{\text{features}} \}.$$

The reward is the same as subsection III-A. The two graphs have the same topology, i.e., the same adjacent matrix. The only difference lies in the feature of user vertexes.

IV. HETEROGENEOUS GNNs FOR THE DDPG ALGORITHM

In this section, we first analyze the PE and PI properties of the policy function and action-value function to be learned by DDPG for the predictive power allocation. Then, we construct GNNs that can learn the two functions with the desired properties.

A. PE and PI Properties of the Two Functions

A multivariate function $\mathbf{y} = f(\mathbf{X})$ is one-dimension (1D)-PE, 1D-PI, two-dimension (2D)-PE, and 2D-PI to \mathbf{X} if $\Pi_1 \mathbf{y} = f(\Pi_1 \mathbf{X})$, $\mathbf{y} = f(\Pi_1 \mathbf{X})$, $\Pi_1 \mathbf{y} = f(\Pi_1 \mathbf{X} \Pi_2^\top)$, and $\mathbf{y} = f(\Pi_1 \mathbf{X} \Pi_2^\top)$, respectively, where Π_1 and Π_2 are permutation matrices [27, 35].

Denote the *policy function* to be learned by the actor network as $\tilde{\mu}(\cdot)$, which maps the state graph into the action, i.e., $\mathbf{a}_t = \tilde{\mu}(\{\mathcal{U}, \mathcal{B}\}, \mathcal{E}, \{\mathbf{U}_t, \mathbf{b}_t, \mathbf{E}_t\})$. If we permute the user vertexes, then the elements in \mathbf{a}_t , the rows of \mathbf{U}_t and \mathbf{E}_t will be permuted in the same way, while the policy function will not be changed. If we permute the DU vertexes, then the elements in \mathbf{b}_t and columns of \mathbf{E}_t will be permuted in the same way, whereas the policy function remains unchanged. Hence, $\tilde{\mu}(\cdot)$ is 1D-PE to \mathbf{U}_t , 1D-PI to \mathbf{b}_t , and 2D-PE to \mathbf{E}_t .

Denote the *action-value function* to be learned by the critic network as $\tilde{Q}(\cdot)$, which maps the state-action graph into expected return $q \triangleq \mathbb{E}[\sum_{i=t}^{(N_v-1)N_f} \gamma r_i]$, i.e., $q = \tilde{Q}(\{\mathcal{U}, \mathcal{B}\}, \mathcal{E}, \{\tilde{\mathbf{U}}_t, \mathbf{b}_t, \mathbf{E}_t\})$, where γ is the discount factor. The expected return will remain unchanged if the order of the user or DU vertexes changes. Hence, $\tilde{Q}(\cdot)$ is 1D-PI to \mathbf{U}_t and \mathbf{b}_t , and 2D-PI to \mathbf{E}_t .

The properties of the policy and the action-value functions can be respectively expressed as,

$$\Pi_1 \mathbf{a}_t = \tilde{\mu}(\{\mathcal{U}, \mathcal{B}\}, \mathcal{E}, \{\Pi_1 \mathbf{U}_t, \Pi_2 \mathbf{b}_t, \Pi_1 \mathbf{E}_t \Pi_2^\top\}), \quad (8a)$$

$$q = \tilde{Q}(\{\mathcal{U}, \mathcal{B}\}, \mathcal{E}, \{\Pi_1 \tilde{\mathbf{U}}_t, \Pi_2 \mathbf{b}_t, \Pi_1 \mathbf{E}_t \Pi_2^\top\}). \quad (8b)$$

B. Designing Heterogeneous GNN to Satisfy the PE and PI Properties

Both the state graph and state-action graph consist of two types of vertexes, i.e., user vertex and DU vertex, and hence are heterogeneous graphs. Heterogeneous GNN (called GNN for short) can be used to learn on heterogeneous graph, where the output of the m th vertex at time step t in each layer of the GNN can be obtained with the following two steps [36].

- **Aggregation:** Denote $\mathcal{N}_{t,a}(m)$ as the set of vertexes of the a th type neighboring to the m th vertex at time step t . In the l th layer, the hidden output of the vertexes in $\mathcal{N}_{t,a}(m)$ in previous layer are aggregated at the m th vertex as,

$$\mathbf{d}'_{t,m,a} = \text{PL}_{m,n \in \mathcal{N}_{t,a}(m)}(q_{m,n}(\mathbf{d}_{t,n}^{(l-1)}, \mathbf{e}_{t,m}^n, \boldsymbol{\phi}_{m,n}^{(l)})), \quad (9)$$

where $\mathbf{d}_{t,n}^{(l-1)}$ is the hidden output of the n th vertex in the $(l-1)$ th layer and $\mathbf{e}_{t,m}^n$ is the feature of edge between the m th vertex and the n th vertex, $q_{m,n}(\cdot, \cdot, \boldsymbol{\phi}_{m,n}^{(l)})$ is used to process the features of vertexes and edges with model parameters $\boldsymbol{\phi}_{m,n}^{(l)}$, $\text{PL}_{m,n \in \mathcal{N}_{t,a}(m)}(\cdot)$ is the pooling function to aggregate information from neighboring vertexes of the a th type and edges.

- **Combination:** The output of the m th vertex in the l th layer can be obtained as,

$$\mathbf{d}_{t,m}^{(l)} = \text{CB}_m(\mathbf{d}_{t,m}^{(l-1)}, \{\mathbf{d}'_{t,m,a}^{(l)}, a \in \mathcal{A}\}, \boldsymbol{\theta}_m^{(l)}), \quad (10)$$

where $\text{CB}_m(\cdot, \cdot, \boldsymbol{\theta}_m^{(l)})$ is a combiner with model parameters $\boldsymbol{\theta}_m^{(l)}$, and \mathcal{A} is the set of vertex types (e.g., $\mathcal{A} = \{1, 2\}$ for the considered problem).

GNN can be used for graph embedding or for learning a policy in an end-to-end manner. In the following, we show how to construct the actor and critic networks with GNNs to learn the functions with desired PE and PI properties in two manners.

1) *Design of actor and critic networks with GNN for embedding:* A GNN used for graph embedding maps a graph into vector representations by extracting the information of graph topology and vertex/edge features. To learn a policy, extra layers are required to map the vector representations into the outputs of the policy. For graph-based DDPG, both actor and critic networks are composed of a GNN and output layers. Since the state graph and state-action graph only differ in the feature of user vertexes, the GNNs for actor network and critic network have the same structure but differ in features of the graph. To satisfy the properties in (8), the GNN as well as the output layers of each neural network should be designed judiciously.

When we permute the vertexes with the same type in a graph, relevant feature matrixes are permuted accordingly but the topology of the graph remains unchanged. Taking the state graph

as an example as illustrated in Fig. 2, when we permute two user vertexes, the feature matrixes of user vertexes and edges are permuted while the feature matrixes of DU vertexes are same.

This suggests that a GNN used for graph embedding satisfies the following property.

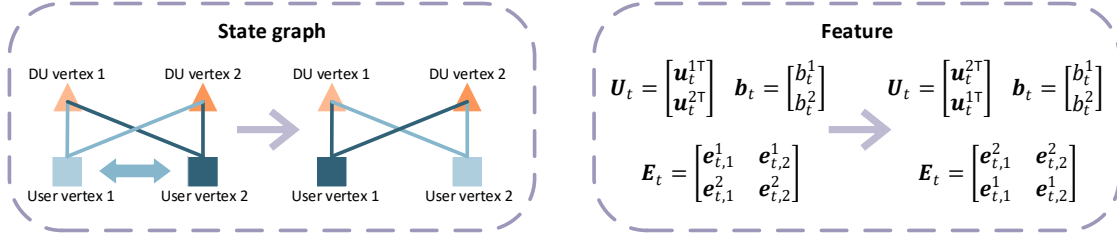


Fig. 2. Permutation of user vertexes in the state graph.

Property 1: *When the vertexes with the same type in a graph are permuted, (a) the vector representations of these vertexes after embedding are permuted in the same way, (b) the vector representations of all other vertexes after embedding do not change.*

The following proposition provides a principle for designing a GNN to satisfy Property 1.

Proposition 1: The GNN will satisfy Property 1 if the processor, pooling function and combiner in (9) and (10) satisfy the following conditions: (1) $q_{m,n}(\cdot, \cdot, \phi_{m,n}^{(l)})$ is identical for the vertexes with the same type when they are aggregated at the vertexes with the same type, (2) $PL_{m,n \in \mathcal{N}_{t,a}(m)}(\cdot)$ and $CB_m(\cdot, \cdot, \theta_m^{(l)})$ are identical for all the vertexes with the same type, and (3) $PL_{m,n \in \mathcal{N}_{t,a}(m)}(\cdot)$ satisfies commutative law.

Proof: See Appendix A. ■

There are a variety of choices for the processor, pooling function and combiner [31]. For easy understanding, we choose $q_{m,n}(\cdot, \cdot, \phi_{m,n}^{(l)})$ as linear processor, and $CB_m(\cdot, \cdot, \theta_m^{(l)})$ as linear processor followed by an activation function, for illustrating how to design a GNN for satisfying Property 1. Since there are only two types of vertexes in our problem, we remove type subscript a for notational simplicity in the sequel.

To satisfy the condition (1) in Proposition 1, we use the same model parameters $\{\mathbf{V}_1^{(l)}, \mathbf{V}_2^{(l)}\}$ for the processor $q(\cdot)$ when every DU vertex aggregates information from user vertexes, and $\{\mathbf{Y}_1^{(l)}, \mathbf{Y}_2^{(l)}\}$ for $q(\cdot)$ when every user vertex aggregates information from DU vertexes. To satisfy the condition (2), we use the same model parameters $\mathbf{V}_3^{(l)}$ in combiner $CB(\cdot)$ for all DU vertexes and $\mathbf{Y}_3^{(l)}$ in $CB(\cdot)$ for all user vertexes, and use the same pooling function for all the DU and user vertexes. To satisfy the condition (3), we choose pooling function as summation.

Denote the output of the m th DU vertex and the k th user vertex in the l th layer at time step t of the GNN as $\mathbf{b}_{t,m}^{(l)}$ and $\mathbf{u}_{t,k}^{(l)}$, respectively. Then, the update equation for the GNN constructed to satisfy Property 1 can be expressed as follows:

DUs aggregating information from Users

$$\text{Aggregate : } \mathbf{b}'_{t,m}{}^{(l)} = \sum_{k=1}^K \left(\mathbf{V}_1^{(l)} \mathbf{u}_{t,k}^{(l-1)} + \mathbf{V}_2^{(l)} \mathbf{e}_{t,m}^k \right), \quad (11a)$$

$$\text{Combine : } \mathbf{b}_{t,m}^{(l)} = \sigma \left(\mathbf{V}_3^{(l)} \mathbf{b}_{t,m}^{(l-1)} + \mathbf{b}'_{t,m}{}^{(l)} \right), m = 1 \cdots, M,$$

Users aggregating information from DUs

$$\text{Aggregate : } \mathbf{u}'_{t,k}{}^{(l)} = \sum_{m=1}^M \left(\mathbf{Y}_1^{(l)} \mathbf{b}_{t,m}^{(l-1)} + \mathbf{Y}_2^{(l)} \mathbf{e}_{t,k}^m \right), \quad (11b)$$

$$\text{Combine : } \mathbf{u}_{t,k}^{(l)} = \sigma \left(\mathbf{Y}_3^{(l)} \mathbf{u}_{t,k}^{(l-1)} + \mathbf{u}'_{t,k}{}^{(l)} \right), k = 1 \cdots, K,$$

where $\sigma(\cdot)$ is an activation function, $\mathbf{e}_{t,m}^k$ is the feature vector of the edge between the m th DU vertex and the k th user vertex defined in (7), and $\mathbf{b}_{t,m}^{(0)}$ and $\mathbf{u}_{t,k}^{(0)}$ are the inputs of each GNN. In particular, $\mathbf{b}_{t,m}^{(0)} = b_t^m$ and $\mathbf{u}_{t,k}^{(0)} = \mathbf{u}_t^k$ in the GNN for actor network, and $\mathbf{b}_{t,m}^{(0)} = b_t^m$ and $\mathbf{u}_{t,k}^{(0)} = \tilde{\mathbf{u}}_t^k$ in the GNN for critic network.

The resulting parameter sharing in the weighting matrix between layers can be observed by rewriting (11) as

$$\begin{aligned} \begin{bmatrix} \mathbf{b}_{t,1}^{(l)\top} \\ \vdots \\ \mathbf{b}_{t,M}^{(l)\top} \\ \mathbf{u}_{t,1}^{(l)\top} \\ \vdots \\ \mathbf{u}_{t,K}^{(l)\top} \end{bmatrix} &= \sigma \left(\begin{bmatrix} \mathbf{V}_3^{(l)} & \cdots & 0 & 0 & \cdots & 0 \\ \vdots & \ddots & \vdots & \vdots & \ddots & \vdots \\ 0 & \cdots & \mathbf{V}_3^{(l)} & 0 & \cdots & 0 \\ 0 & \cdots & 0 & \mathbf{Y}_3^{(l)} & \cdots & 0 \\ \vdots & \ddots & \vdots & \vdots & \ddots & \vdots \\ 0 & \cdots & 0 & 0 & \cdots & \mathbf{Y}_3^{(l)} \end{bmatrix} \begin{bmatrix} \mathbf{b}_{t,1}^{(l-1)\top} \\ \vdots \\ \mathbf{b}_{t,M}^{(l-1)\top} \\ \mathbf{u}_{t,1}^{(l-1)\top} \\ \vdots \\ \mathbf{u}_{t,K}^{(l-1)\top} \end{bmatrix} + \begin{bmatrix} 0 & \cdots & 0 & \mathbf{V}_1^{(l)} & \cdots & \mathbf{V}_1^{(l)} \\ \vdots & \ddots & \vdots & \vdots & \ddots & \vdots \\ 0 & \cdots & 0 & \mathbf{V}_1^{(l)} & \cdots & \mathbf{V}_1^{(l)} \\ \mathbf{Y}_1^{(l)} & \cdots & \mathbf{Y}_1^{(l)} & 0 & \cdots & 0 \\ \vdots & \ddots & \vdots & \vdots & \ddots & \vdots \\ \mathbf{Y}_1^{(l)} & \cdots & \mathbf{Y}_1^{(l)} & 0 & \cdots & 0 \end{bmatrix} \begin{bmatrix} \mathbf{b}_{t,1}^{(l-1)\top} \\ \vdots \\ \mathbf{b}_{t,M}^{(l-1)\top} \\ \mathbf{u}_{t,1}^{(l-1)\top} \\ \vdots \\ \mathbf{u}_{t,K}^{(l-1)\top} \end{bmatrix} \right. \\ &\quad \left. + \begin{bmatrix} 0 & \cdots & 0 & \mathbf{e}_{t,1}^1 & \cdots & \mathbf{e}_{t,1}^K \\ \vdots & \ddots & \vdots & \vdots & \ddots & \vdots \\ 0 & \cdots & 0 & \mathbf{e}_{t,M}^1 & \cdots & \mathbf{e}_{t,M}^K \\ \mathbf{e}_{t,1}^1 & \cdots & \mathbf{e}_{t,M}^1 & 0 & \cdots & 0 \\ \vdots & \ddots & \vdots & \vdots & \ddots & \vdots \\ \mathbf{e}_{t,1}^K & \cdots & \mathbf{e}_{t,M}^K & 0 & \cdots & 0 \end{bmatrix} \begin{bmatrix} \mathbf{Y}_2^{(l)} \\ \vdots \\ \mathbf{Y}_2^{(l)} \\ \mathbf{V}_2^{(l)} \\ \vdots \\ \mathbf{V}_2^{(l)} \end{bmatrix} \right). \quad (12) \end{aligned}$$

Denote $\mathbf{B}_t^{(l)} \triangleq [\mathbf{b}_{t,1}^{(l)}, \dots, \mathbf{b}_{t,M}^{(l)}]^\top$ and $\mathbf{U}_t^{(l)} \triangleq [\mathbf{u}_{t,1}^{(l)}, \dots, \mathbf{u}_{t,K}^{(l)}]^\top$. For notational simplicity, we do not differentiate the GNNs for the actor and critic networks and assume that both GNNs have L layers. Then, the vector representations of all DU vertexes and all user vertexes are $\mathbf{B}_t^{(L)}$ and $\mathbf{U}_t^{(L)}$, respectively. From Proposition 1, it is not hard to obtain the following corollary.

Corollary 1: For the GNN with update equation in (11), $\mathbf{U}_t^{(L)}$ is 1D-PE to \mathbf{U}_t , 1D-PI to \mathbf{b}_t , and 2D-PE to \mathbf{E}_t , while $\mathbf{B}_t^{(L)}$ is 1D-PI to \mathbf{U}_t , 1D-PE to \mathbf{b}_t , and 2D-PE to \mathbf{E}_t^\top .

To learn the mapping from the vector representations to the action or expected return, the GNNs should be cascaded with output layers satisfying the desirable properties in (8).

Both the action \mathbf{a}_t and $\mathbf{U}_t^{(L)}$ are 1D-PE to \mathbf{U}_t . If we permute \mathbf{U}_t into $\Pi_1 \mathbf{U}_t$, then \mathbf{a}_t and $\mathbf{U}_t^{(L)}$ are permuted into $\Pi_1 \mathbf{a}_t$ and $\Pi_1 \mathbf{U}_t^{(L)}$. Hence, \mathbf{a}_t is 1D-PE to $\mathbf{U}_t^{(L)}$. It is not hard to show that \mathbf{a}_t is 1D-PI to $\mathbf{B}_t^{(L)}$. Therefore, the output layer of the actor network can be designed as

$$\mathbf{a}_t = \xi_1 \text{PENN}(\mathbf{U}_t^{(L)}) + \xi_2 \text{PINN}(\mathbf{B}_t^{(L)}), \quad (13)$$

where ξ_1 and ξ_2 are hyper-parameters, $\text{PENN}(\cdot)$ is a 1D-PENN that can learn the functions with 1D-PE property, whose weighting matrix in each layer are with identical sub-matrices on the diagonal and non-diagonal positions, respectively, and $\text{PINN}(\cdot)$ is a 1D-PINN, whose weighting matrix is a row block matrix with identical sub-matrices [27, 35].

Finally, the structure of the *actor network* is shown in Fig. 3(a). If the output of actor network does not satisfy the constraint in (1b), we can adjust the action using (5). It is easy to verify that such an adjustment does not affect the permutational property of the actor network.

It is not hard to show that the expected return q is 1D-PI to $\mathbf{U}_t^{(L)}$ and 1D-PI to $\mathbf{B}_t^{(L)}$. Thereby, the output layer of the critic network can be designed as

$$q = \lambda_1 \text{PINN}_1(\mathbf{U}_t^{(L)}) + \lambda_2 \text{PINN}_2(\mathbf{B}_t^{(L)}), \quad (14)$$

where λ_1 and λ_2 are hyper-parameters, and $\text{PINN}_1(\cdot)$ and $\text{PINN}_2(\cdot)$ are 1D-PINNs.

Then, the structure of the *critic network* is shown in Fig. 3(b).

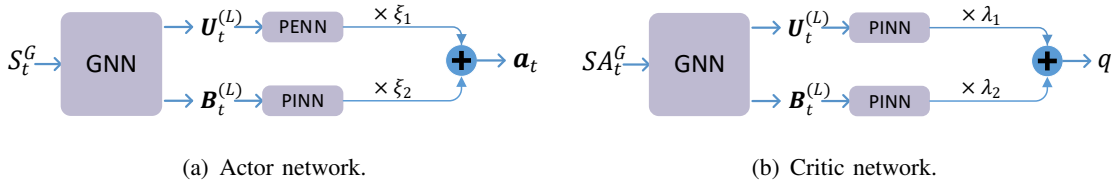


Fig. 3. Structure of the actor and critic networks using GNN in embedding manner.

Based on Proposition 1, (13), and (14), we can obtain the following corollary.

Corollary 2: The output of the actor network is 1D-PE to \mathbf{U}_t , 1D-PI to \mathbf{b}_t , and 2D-PE to \mathbf{E}_t . The output of the critic network is 1D-PI to $\tilde{\mathbf{U}}_t$, 1D-PI to \mathbf{b}_t , and 2D-PI to \mathbf{E}_t .

2) *Design of actor and critic networks using GNN in end-to-end manner:* If we set the output dimension for each vertex as one and let $\mathbf{a}_t = \mathbf{U}_t^{(L)}$, then the GNN in (11) can be used as the actor network, whose input is S_t^G and output is \mathbf{a}_t . According to Corollary 1, the GNN satisfies

the properties in (8a). Again, we need to adjust the action as (5) if the output of actor network does not satisfy the constraint in (1b).

If we set the output dimension for each vertex as one and let $q = \lambda'_1 \sum_{k=1}^K \mathbf{u}_{t,k}^{(L)} + \lambda'_2 \sum_{m=1}^M \mathbf{b}_{t,m}^{(L)}$, then the GNN in (11) can be used as the critic network, whose input is SA_t^G and output is q , where λ'_1 and λ'_2 are hyper-parameters. It is easy to show that the GNN satisfies the properties in (8b).

3) *Batch normalization*: To accelerate learning, batch normalization (BN) should be applied to normalize the input to the activation function in each layer for each batch [32]. In what follows, we show that the vanilla BN method proposed in [32] destroys the PE and PI properties. Then, we introduce a method for batch normalization for permutable samples.

The outputs in each hidden layer of the GNN, e.g., $\mathbf{U}_t^{(l)}$, are matrices. Hence, each sample in a batch for computing gradient can be expressed as a matrix. Since all samples in a batch are from the same layer, we omit superscript l for notational simplicity. Denote a batch of hidden outputs in the l th layer of all user vertexes as \mathcal{B}_s , the b th sample in \mathcal{B}_s as $\mathbf{U}^{}$, and the hidden output of the k th user in $\mathbf{U}^{}$ as $\mathbf{u}_k^{}$. Denote $u_{k,i}^{}$ as the i th element in $\mathbf{u}_k^{}$.

For easy understanding, we consider a batch that contains three samples, and each is the hidden outputs of two users in a GNN. Then, the b th sample in \mathcal{B}_s can be expressed as,

$$\mathbf{U}^{} = \begin{bmatrix} \mathbf{u}_1^{} \\ \mathbf{u}_2^{} \end{bmatrix} = \begin{bmatrix} u_{1,1}^{} & \cdots & u_{1,i}^{} & \cdots \\ u_{2,1}^{} & \cdots & u_{2,i}^{} & \cdots \end{bmatrix}, \quad (15a)$$

and the batch can be expressed as

$$\mathcal{B}_s = \begin{bmatrix} \mathbf{U}^{<1>} \\ \mathbf{U}^{<2>} \\ \mathbf{U}^{<3>} \end{bmatrix} = \begin{bmatrix} u_{1,1}^{<1>} & \cdots & u_{1,i}^{<1>} & \cdots \\ u_{2,1}^{<1>} & \cdots & u_{2,i}^{<1>} & \cdots \\ \hline u_{1,1}^{<2>} & \cdots & u_{1,i}^{<2>} & \cdots \\ u_{2,1}^{<2>} & \cdots & u_{2,i}^{<2>} & \cdots \\ \hline u_{1,1}^{<3>} & \cdots & u_{1,i}^{<3>} & \cdots \\ u_{2,1}^{<3>} & \cdots & u_{2,i}^{<3>} & \cdots \end{bmatrix}. \quad (16)$$

The vanilla BN method in [32] normalizes each scalar feature in the samples independently by estimating the mean and variance of the feature in samples. For example, $u_{1,1}^{<1>}$ is normalized by the mean and variance of $u_{1,1}^{<1>}$, $u_{1,1}^{<2>}$ and $u_{1,1}^{<3>}$ in the three samples as $\hat{u}_{1,1}^{<1>} = \frac{u_{1,1}^{<1>} - M_{1,1}}{\sqrt{V_{1,1}}}$, where $M_{1,1} = \frac{\sum_{b=1}^3 u_{1,1}^{}}{3}$, and $V_{1,1} = \frac{\sum_{b=1}^3 (u_{1,1}^{} - M_{1,1})^2}{3}$.

If we change the order of users in $\mathbf{U}^{<1>}$, then the batch in (16) becomes,

$$\mathcal{B}'_s = \begin{bmatrix} \mathbf{U}'^{<1>} \\ \mathbf{U}^{<2>} \\ \mathbf{U}^{<3>} \end{bmatrix} = \begin{bmatrix} u_{2,1}^{<1>} & \cdots & u_{2,i}^{<1>} & \cdots \\ u_{1,1}^{<1>} & \cdots & u_{1,i}^{<1>} & \cdots \\ \hline u_{1,1}^{<2>} & \cdots & u_{1,i}^{<2>} & \cdots \\ u_{2,1}^{<2>} & \cdots & u_{2,i}^{<2>} & \cdots \\ \hline u_{1,1}^{<3>} & \cdots & u_{1,i}^{<3>} & \cdots \\ u_{2,1}^{<3>} & \cdots & u_{2,i}^{<3>} & \cdots \end{bmatrix}. \quad (17)$$

When using the vanilla batch normalization, the mean $M'_{1,1}$ and variance $V'_{1,1}$ for normalizing $u_{1,1}^{<1>}$ are computed as

$$M'_{1,1} = \frac{u_{1,1}^{<1>} + u_{2,1}^{<2>} + u_{2,1}^{<3>}}{3}, \quad V'_{1,1} = \frac{\sum_{b=2}^3 (u_{2,1}^{} - M'_{1,1})^2 + (u_{1,1}^{<1>} - M'_{1,1})^2}{3}. \quad (18)$$

Then, the normalized output of $u_{1,1}^{<1>}$ becomes $\hat{u}'_{1,1} = \frac{u_{1,1}^{<1>} - M'_{1,1}}{\sqrt{V'_{1,1}}} \neq \hat{u}_{1,1}^{<1>}$, i.e., the permutation properties will no longer satisfy.

To support the permutation properties, we design a method for batch normalization, which jointly normalizes all features that can be permuted with each other. In the considered example, $u_{1,1}^{}$ and $u_{2,1}^{}$ are permutable for $\forall b = 1, 2, 3$ in \mathcal{B}_s . Hence, $\{u_{1,1}^{<1>}, u_{2,1}^{<1>}, u_{1,1}^{<2>}, u_{2,1}^{<2>}, u_{1,1}^{<3>}, u_{2,1}^{<3>}\}$ are normalized together, and their mean and variance are respectively

$$M^* = \frac{\sum_{b=1}^3 \sum_{j=1}^2 u_{j,1}^{}}{6}, \quad V^* = \frac{\sum_{b=1}^3 \sum_{j=1}^2 (u_{j,1}^{} - M^*)^2}{6}. \quad (19)$$

Then, the values of normalized outputs for $u_{1,1}^{<1>}$ in \mathcal{B}_s and \mathcal{B}'_s are identical. We can see that the normalized outputs are 1D-PE to the inputs.

V. PE/PI-DNNs FOR THE DDPG ALGORITHM

In this section, we construct PE/PI-DNNs for actor and critic networks satisfying the desired permutational properties, where the state and action are respectively represented as matrix and vector as in section III-A, and compare with GNNs.

A. Constructing PE/PI-DNNs to Satisfy the Properties

The actor network learns the mapping from the state matrix \mathbf{S}_t to the action vector \mathbf{a}_t . When the order of users changes, the order of the elements in \mathbf{a}_t and the rows of \mathbf{S}_t change in the same way while the policy function remains unchanged. Since \mathbf{a}_t is 1D-PE to \mathbf{S}_t as analyzed in section IV-A, the actor network can be constructed as a 1D-PENN. The hidden output of the k th user in the l th layer in the PENN at time step t can be updated as [35],

$$\mathbf{u}_{t,k}^{(l)} = \sigma \left(\mathbf{P}_1^{(l)} \mathbf{u}_{t,k}^{(l-1)} + \sum_{i=1, i \neq k}^K \mathbf{P}_2^{(l)} \mathbf{u}_{t,i}^{(l-1)} \right), \quad (20)$$

where $\mathbf{P}_1^{(l)}$ and $\mathbf{P}_2^{(l)}$ are the model parameters, and $\mathbf{u}_{t,k}^{(0)} = \mathbf{s}_t^k$, which defined in (3).

To observe the parameter sharing in the weighting matrix between layers of the PENN, we rewrite (20) in matrix form as

$$\begin{bmatrix} \mathbf{u}_{t,1}^{(l)\top} \\ \mathbf{u}_{t,2}^{(l)\top} \\ \vdots \\ \mathbf{u}_{t,K}^{(l)\top} \end{bmatrix} = \sigma \left(\begin{bmatrix} \mathbf{P}_1^{(l)} & 0 & \cdots & 0 \\ 0 & \mathbf{P}_1^{(l)} & \cdots & 0 \\ \vdots & \vdots & \ddots & \vdots \\ 0 & 0 & \cdots & \mathbf{P}_1^{(l)} \end{bmatrix} \begin{bmatrix} \mathbf{u}_{t,1}^{(l-1)\top} \\ \mathbf{u}_{t,2}^{(l-1)\top} \\ \vdots \\ \mathbf{u}_{t,K}^{(l-1)\top} \end{bmatrix} + \begin{bmatrix} 0 & \mathbf{P}_2^{(l)} & \cdots & \mathbf{P}_2^{(l)} \\ \mathbf{P}_2^{(l)} & 0 & \cdots & \mathbf{P}_2^{(l)} \\ \vdots & \vdots & \ddots & \vdots \\ \mathbf{P}_2^{(l)} & \mathbf{P}_2^{(l)} & \cdots & 0 \end{bmatrix} \begin{bmatrix} \mathbf{u}_{t,1}^{(l-1)\top} \\ \mathbf{u}_{t,2}^{(l-1)\top} \\ \vdots \\ \mathbf{u}_{t,K}^{(l-1)\top} \end{bmatrix} \right). \quad (21)$$

The critic network learns the mapping from \mathbf{S}_t and \mathbf{a}_t into q . By stacking the state and action according to the indexes of users, the state-action pair of the k th user can be expressed as

$$\mathbf{s}\mathbf{a}_t^k \triangleq [B_t^k, l_t^k, \eta_t^k, M_t^k, \boldsymbol{\alpha}_{t-T}^{k\top}, \dots, \boldsymbol{\alpha}_t^{k\top}, \bar{R}_t^k]^\top. \quad (22)$$

Then, the state-action matrix is $\mathbf{S}\mathbf{a}_t = [\mathbf{s}\mathbf{a}_t^1, \dots, \mathbf{s}\mathbf{a}_t^K]^\top$. We can see that the expected return will remain unchanged if the order of users in the state-action matrix changes. Since q is 1D-PI to $\mathbf{S}\mathbf{a}_t$ as analyzed in section IV-A, the critic network can be constructed as a 1D-PINN. For the k th user, at time step t the output of hidden layers of the 1D-PINN can be updated with (20), while the output layer in the PINN is updated as [35],

$$\mathbf{u}_{t,k}^{(l)} = \sigma \left(\sum_{i=1}^K \mathbf{Q}_k^{(l)} \mathbf{u}_{t,i}^{(l-1)} \right), \quad (23)$$

where $\mathbf{Q}_k^{(l)}$ is the model parameters.

B. Comparing PE/PINNs with GNNs

Both the constructed GNNs and PE/PINNs can exploit the permutational properties, while GNNs can also harness another kind of prior: relationship among vertexes. To see this, we take the GNN used in the embedding manner for actor network as an example.

The relationship among DUs and users is *implicitly* reflected in the state matrix, i.e., M_t^k , which however does not affect the weight matrices of the PE/PINNs. This is because PE/PINNs are designed by introducing parameter sharing into FNNs to satisfy the PE/PI properties [35].

The relationship among DU and user vertexes is *explicitly* reflected by the edges in the state graph, which affects the weight matrices of the GNN. The parameter sharing in the GNN comes from designing a GNN to satisfy Property 1 of heterogeneous GNNs, which depends on the graph topology and implies the permutational properties.

By comparing the weight matrices of GNN and PENN, we can see that the first term in the right hand side (r.h.s.) of (12) and (21) has the same structure (both are block diagonal

matrices), but there are two submatrices $\mathbf{V}_3^{(l)}$ and $\mathbf{Y}_3^{(l)}$ in GNN that are respectively used for the combination at the two types of vertexes. The second term in the r.h.s. of (12) can be regarded as having been multiplied with the adjacent matrix in Fig. 1 with Hadamard product, which reflects the aggregation only from adjacent vertexes (i.e., the vertexes with edges). The third term in the r.h.s. of (12) reflects the aggregation from the edges with adjacent vertexes.

In Fig. 4, we illustrate the structures of 1D-PENN and GNN, where $M = 2$, $K = 2$, and each DU is associated with a single user. In order not to make the figure too complicated to see the difference between the structures, we do not show the connection between each neuron and each edge. In the PENN, all neurons are connected to all neurons, while in the GNN only the neurons for the vertexes with edges are connected. For example, user vertex 1 has no edge with user vertex 2, hence its hidden output in the l th layer is obtained without using the hidden outputs of user vertex 2 in the $(l - 1)$ th layer.

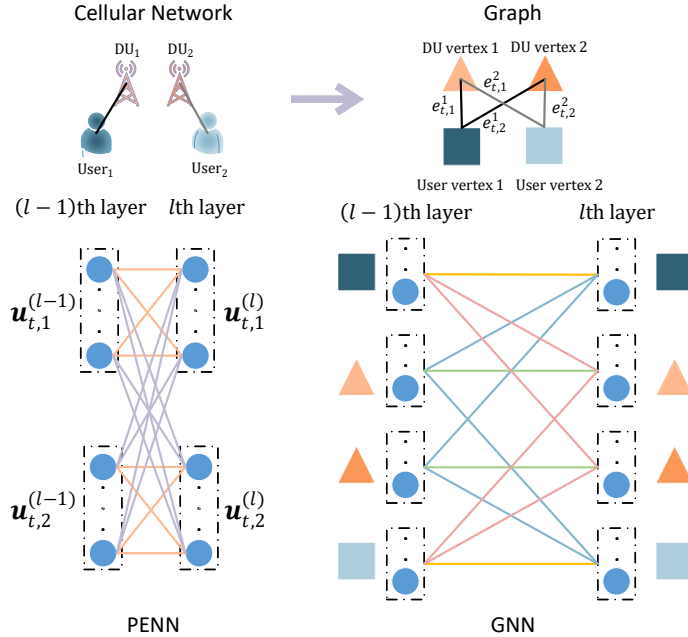


Fig. 4. Structure of 1D-PENN and GNN for actor network. The circles represent neurons. The connection among neurons with the same color are with identical sub-weight matrices. We do not show the edges in GNN for clarity.

VI. SIMULATION RESULTS

In this section, we evaluate the performance of the graph-based DRL algorithms and show the gain from harnessing priors in terms of convergence speed, model size, as well as the computing time and signaling overhead for training.

To this end, we compare the following algorithms.

1) “*Optimal*”: This is the optimal solution of problem (1) assuming perfect future large-scale channel gains [19], which serves as the performance upper bound for learning-based solutions.

2) “*GNN-DDPG*”: This is the DDPG using the GNN in end-to-end manner designed in section IV-B, where the BN method designed in section IV-B3 is used.

3) “*GNN-DDPG+PE/PINN*”: This is the DDPG using the GNN in embedding manner designed in section IV-B, where the BN method designed in section IV-B3 is used.

4) “*GNN-DDPG+FNN*”: This is the DDPG using the GNN in embedding manner, but both actor and critic networks in DDPG are GNNs each using a FNN as output layer analogous to the graph deep Q-network in [28], which do not satisfy the properties in (8). We use the BN method designed in section IV-B3 to ensure the properties only for GNNs.

5) “*GNN-DDPG+PE/PINN with vanilla BN*”: The only difference of this algorithm from “*GNN-DDPG+PE/PINN*” is that the vanilla BN method is used here. Hence, the properties in (8) are no longer satisfied.

6) “*PE/PINN-DDPG*”: This is the DDPG in section V-A, where the actor network is a PENN and the critic network is a PINN, and the BN method designed in section IV-B3 is used.

7) “*FNN-DDPG*”: This is the DDPG with FNNs [33], which uses the DRL framework in section III-A and employs the vanilla BN method in [32].

In Table I, we summarize the relational priors exploited in these algorithms.

TABLE I
RELATIONAL PRIORS EXPLOITED IN EACH DDPG ALGORITHM.

	FNN-DDPG	GNN-DDPG	GNN-DDPG+PE/PINN	GNN-DDPG+FNN	PE/PINN-DDPG	GNN-DDPG+PE/PINN with vanilla BN
PE/PI properties of task functions	✗	✓	✓	✗	✓	✗
Relations among vertexes	✗	✓	✓	✓	✗	✓

A. Simulation Setup

Consider a scenario shown in Fig. 5, where K users move along roads across cells. The inter-DU distance is 500 m [37], the maximal transmit power and the number of antennas of each DU is 200 W and 64, respectively. The path loss is modeled as $13.54 + 39.08 \log_{10}(d) + 20 \log_{10}(f_c)$ in dB, where d is the distance between user and DU in meters, f_c is the carrier frequency and is set as 3.5 GHz [37]. The small-scale channels follow Rayleigh fading. The noise spectral density is -174 dBm/Hz. The bandwidth assigned for each user is 2 MHz.

The playback duration of each video and each segment is 150 s and 10 s, respectively. Each segment is with size of 8 Mbps [38]. Each time frame is with duration of $\Delta T = 1$ s, and each time slot is with duration of $\tau = 1$ ms (hence $N_s = 1000$).

The trajectory of each user is generated with Bonnmotion software [39], which is commonly applied for vehicular networks, where the trajectory follows Gauss-Markov model. The initial velocity of users is set as 16 m/s, and the minimal and maximal velocities of users are 12 m/s and 20 m/s, respectively. When a user encounters a traffic light, which is red or green with 50% probability, the user may stop 0 ~ 30 seconds if the traffic light is red.

The simulation setup is used in the following unless otherwise specified.

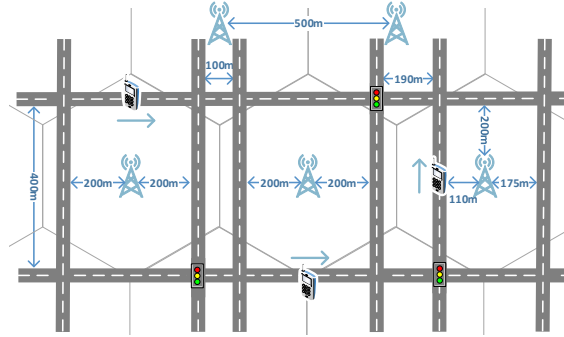


Fig. 5. Simulation scenario, where K users move along roads in five cells.

B. Fine-Tuned Parameters

We set $T = 2$ and $N_b = 2$ in the state. The discount factor $\gamma = 1$. The update rate for the target actor and critic networks is $\omega = 10^{-3}$ [33]. The replay memory size is 10^6 , and the mini-batch size for gradient descent is 1024. The noise term n_t follows Gaussian distribution with zero mean and the variance decreased linearly from 0.1 to 0. We use Adam [40] to optimize the model parameters. For GNN-DDPG+PE/PINN, we set $\xi_1 = 1$ and $\xi_2 = 0$ for PENN in actor network, $\lambda_1 = 1$ and $\lambda_2 = 0$ for PINN in critic network. For GNN-DDPG, we set $\lambda'_1 = 1$ and $\lambda'_2 = 0$ in critic network. The results for other values of these parameters are similar and hence are not provided.

Other fine-tuned hyper-parameters are listed in Table II, where $*_1$ and $*_3$ in $[*_1, *_2, \dots]$ indicate the number of neurons in the first and second layers of a neural network (say GNN, PENN), respectively. Since the number of hidden layers and the number of hidden nodes in each layer of the actor and critic networks are identical for all algorithms, we only list the numbers for one network. Different from FNN and PENN where the number of neurons in hidden layer is

the dimension of the output vector of the whole layer, the number of neurons in hidden layer of each GNN is the dimension of the output vector of each vertex.

TABLE II
HYPER-PARAMETERS OF EACH ALGORITHM.

		FNN-DDPG	GNN-DDPG	GNN-DDPG +PE/PINN	GNN-DDPG +FNN	PE/PINN -DDPG	GNN-DDPG+PE/PINN with vanilla BN
Learning rate of actor network		0.001	0.001	0.001	0.001	0.001	0.001
Learning rate of critic network		0.0001	0.0001	0.0001	0.001	0.0001	0.0001
Number of neurons in each layer and number of layers	$K = 2$	[200, 200]	[128, 128, 1]	[128, 128], [2]	[128, 128], [500]	[200, 200]	[128, 128], [2]
	$K = 5$	[400, 400, 400]	[128, 128, 1]	[128, 128], [5]	[128, 128], [500]	[400, 400]	[128, 128], [5]
	$K = 8$	[600, 600, 600]	[128, 128, 1]	[128, 128], [8]	[128, 128], [500]	[800, 800, 800]	[128, 128], [8]

C. Performance Evaluation

1) *Convergence*: In Fig. 6, we show the learning curves of the DRL algorithms. The negative of the converged return is the minimal total energy consumed at the DUs for all users by the learned policies. In particular, the energy consumed by GNN-DDPG and GNN-DDPG+PE/PINN after convergence is 49.9 Joule. The energy consumed by “Optimal” is 47 Joule. To show the energy saving gain from predicting average channels, we also simulate a non-predictive power allocation policy without using future information in [4], whose energy consumption is 62 Joule.

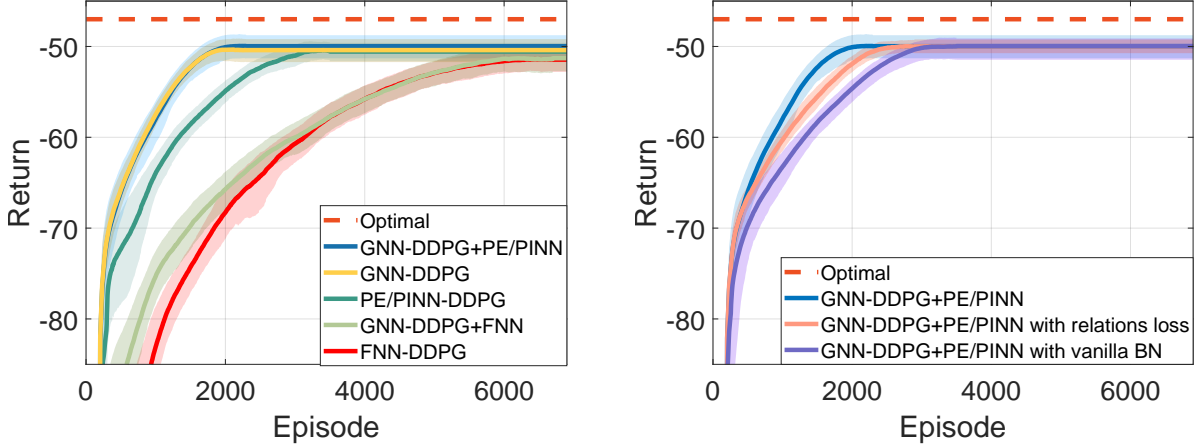
To show the impact of random trajectories on training, we train the DRLs 10 times over 10 Monte-Carlo trials. In each trial, user trajectories are randomly generated with random initial locations, velocities, and stopping times for red traffic lights, and the DRLs are trained from random initial weight matrices. The shadow near the curves is the maximum and minimum returns in the 10 times of training.

In Fig. 6(a), we show the impact of harnessing two kinds of relational priors. We can see that the convergence speeds of GNN-DDPG+PE/PINN and GNN-DDPG are almost the same, both are faster than all the other algorithms. Without exploiting the relation prior among vertex, PE/PINN-DDPG converges slower than GNN-DDPG. Owing to not satisfying the permutational properties after cascading a FNN with GNN, GNN-DDPG+FNN converges much slower than the DDPG algorithms exploiting the properties and only converges faster than FNN-DDPG slightly.

In Fig. 6(b), we show the necessity for designing the graph without relation information loss as mentioned in section III-B3 and for designing batch normalization as mentioned in section IV-B3. It is shown that GNN-DDPG+PE/PINN with vanilla BN converges slower than GNN-DDPG+PE/PINN but achieves almost the same steady return as GNN-DDPG+PE/PINN. To show the impact of information loss illustrated in Fig. 1, we also simulate a GNN-DDPG+PE/PINN

learning over state and state-action graphs where the DU vertexes have no features. We can see that it converges slower than GNN-DDPG+PE/PINN.

By comparing Figs. 6(a) and 6(b), we can see that exploiting the permutational properties dominates the gain of using priors in accelerating convergence.



(a) Impact of using different types of relational priors

(b) Impact of relations loss and batch normalization

Fig. 6. Negative total energy consumption \sim episodes, averaged over 10 Monte Carlo trials and 100 successive episodes, $K = 5$.

2) *Impact of shadowing and number of users*: Since the performance upper bounds and the return depend on channels and number of users, to compare the algorithms in different simulation setups, we consider the performance loss from the upper bound, which is defined as,

$$\text{performance loss} = \left| \frac{\text{Return}_c - \text{Energy}_{op}}{\text{Energy}_{op}} \right|,$$

where Return_c is the return achieved by the DDPG algorithms after convergence, and Energy_{op} is the energy achieved by “Optimal”.

In Fig. 7, we show the impact of shadowing on GNN-DDPG+PE/PINN algorithm, where the large scale channel gains include path loss and shadowing. The shadowing is with standard deviation of 6 dB and correlation distance of 50 m or 100 m [37]. We can see that the performance degrades when considering shadowing, and the degradation is large when the correlation distance is shorter. This is because when the correlation distance decreases, the predicted channel gains are less accurate. Since the shadowing is related to the location of users, the performance increases when the location of each user is added into the features of user vertexes in the state graph and state-action graph (with legend “Shadowing, 100m + location”).

In Fig. 8, we show the scalability of several DDPG algorithms, where the results of the algorithms for different number of users are obtained after convergence (the numbers of required

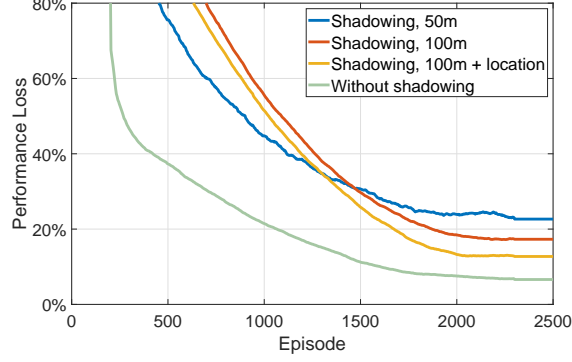


Fig. 7. Impact of shadowing, averaged over 10 Monte Carlo trials and 100 successive episodes, $K = 2$.

episodes are shown on the top of the bars for $K = 2, 6, 10$). Since training FNN+DDPG is too time-consuming, the performance loss for $K > 5$ is obtained from averaging over four trained results. We can see that the performance of graph DRL algorithms remains unchanged and not much more episodes are required for convergence when K increases, but FNN-DDPG performs much worse for more users even with significantly more episodes. This is because the exploration space is reduced by leveraging relational priors. When harnessing the PE and PI properties for designing the actor and critic networks, the permutations of each sample do not affect the policy and reward. Hence, all the permuted samples can also be explored by exploring one sample.

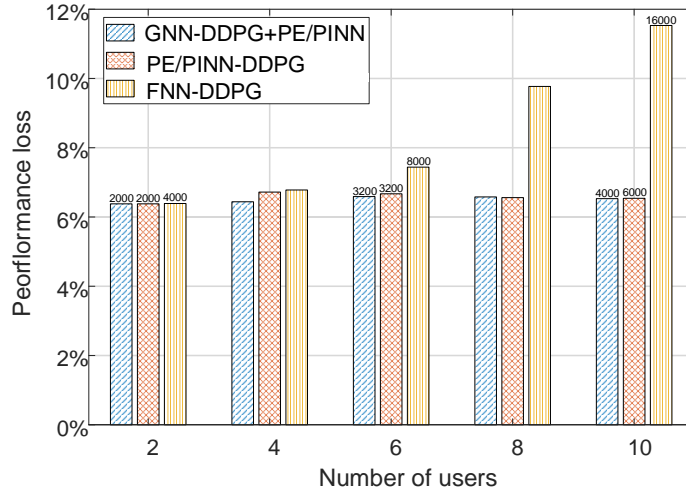


Fig. 8. Scalability of several DDPG algorithms, averaged over Monte Carlo trials, without shadowing.

3) *Training complexity*: In Table III, we compare the training complexity from three aspects.

- **Sample complexity**: It is the minimal number of episodes for converging to an expected performance (set as 10% of the performance loss in the table).
- **Space complexity**: It is the number of free parameters in the DNNs of each DRL algorithm to be trained after fine-tuning.

TABLE III
TRAINING COMPLEXITY FOR 10% PERFORMANCE LOSS.

Training complexity		FNN-DDPG	GNN-DDPG	GNN-DDPG +PE/PINN	GNN-DDPG +FNN	PE/PINN -DDPG	GNN-DDPG+PE/PINN with vanilla BN
$K = 2$	Sample complexity	1400	600	600	1400	1200	1000
	Space complexity	178k	401k	400k	914k	90k	400k
	Time complexity	1.85	0.91	0.70	3.48	0.90	0.86
$K = 5$	Sample complexity	6000	600	600	5600	1600	1000
	Space complexity	1369k	401k	400k	1686k	60k	400k
	Time complexity	8.67	0.96	0.75	11.53	1.68	1.63
$K = 8$	Sample complexity	10000	800	800	7200	4000	1600
	Space complexity	3092k	401k	400k	2456k	169k	400k
	Time complexity	18.27	1.29	1.04	17.10	9.28	2.63

- **Time complexity:** It is the computational time (in hours) consumed for training before converging to an expected performance, which is obtained on a computer with Intel Core™ i9-10940X CPU (3.30GHz) and NVIDIA GeForce RTX 3080 GPU.

We can see that the gain of exploiting priors in terms of reducing training complexity grows with K . By further exploiting the prior of the relation among vertexes, GNN-DDPG or GNN-DDPG+PE/PINN is with much lower sample complexity and time complexity but higher space complexity than PE/PINN-DDPG. When $K = 8$, GNN-DDPG+PE/PINN converges 12 times faster than FNN-DDPG, nine times faster than GNN-DDPG+FNN, five times faster than PE/PINN-DDPG, and two times faster than GNN-DDPG+PE/PINN with vanilla BN. The computing time for training GNN-DDPG+PE/PINN is $\frac{1}{14}$ of FNN-DDPG, $\frac{1}{13}$ of GNN-DDPG+FNN, $\frac{1}{7}$ of PE/PINN-DDPG, and $\frac{1}{2.5}$ of GNN-DDPG+PE/PINN with vanilla BN.

4) *Signaling overhead for training:* Reinforcement learning needs to interact with environment during training, which incurs signaling overhead between DUs and CU. When the DUs are not deployed in the same place with the CU, this overhead generates fronthaul traffic load.

In each time step, each DU sends the state vector of every associated user as well as the consumed energy for the users to the CU in the uplink to compute the reward $\sum_{k=1}^K \sum_{j=1}^{N_s} \tau p_{tj}^k$, and the CU sends action vector to the DUs in the downlink to execute the policy.

For the matrix-based DRL framework in section III-A, the state matrix in (3) contains $10K$ elements ($9K$ real numbers and K integers) for K users when $T = 2$ and $N_b = 2$, the action vector in (2) contains K elements (all real numbers). Therefore, the DUs need to send $(10K + 1)$

decimals to the CU in the uplink, and the CU sends K real numbers to the DU in the downlink in each time step.

For the graph-based DRL framework in section III-B, the DUs can not obtain the state graph or state-action graph, since each DU can only observe the status of associated users. Therefore, each DUs transmits the state vectors of the associated users in each step to the CU. Then, the state matrix of all users is transformed into the state graph with the method in section III-B, and the state-action graph can be obtained from state graph and action vector in the CU. Therefore, the signaling overhead in each time step between the DUs and CU for the graph-based DRL framework is the same as matrix-based DRL framework.

Since the signaling overhead of downlink is far lower than uplink, we only consider uplink. We use b_s bits to quantize each decimal and integer. The signaling overhead for DDPG algorithms in uplink during the training process can be expressed as $(10K + 1) \cdot b_s \cdot T_{total}$, where T_{total} is the number of time steps during the training process.

In Table IV, we compare the uplink signaling overhead of the DDPG algorithms in gigabyte (GB) to achieve 10% performance loss, where $b_s = 32$, $K = 8$ and $M = 5$. To show the connection between signaling overhead and convergence speed, we also provide the sample complexity in Table III for $K = 8$, and list the compression ratio of signaling overhead of other algorithms to GNN-DDPG+PE/PINN algorithm, which is defined as

$$\frac{\text{Signaling overhead of other algorithms}}{\text{Signaling overhead of GNN-DDPG+PE/PINN algorithm}}. \quad (24)$$

The compression ratio of sample complexity is defined in the same way.

Since the number of time steps used for interacting with environment in each episode is random and the value of T_{total} differs among Monte Carlo trials, the signaling overhead is obtained by averaging over four trials. We can see that the signaling overhead of GNN-DDPG+PE/PINN and GNN-DDPG are smaller than all the other algorithms, which is $\frac{1}{12}$ of FNN-DDPG and $\frac{1}{5}$ of PE/PINN-DDPG. The compression ratios of signaling overhead and sample complexity are almost identical. This indicates that faster convergence amounts to lower signaling overhead.

VII. CONCLUSION

In this paper, we established a graph DDPG framework to harness two kinds of relational priors for optimizing predictive power allocation. We showed how to transform the matrix-based DRL framework into graph-based DRL framework. To construct GNNs for learning the policy function and action-value function with desired PI and PE properties, we respectively designed parameter

TABLE IV
SIGNALING OVERHEAD AND SAMPLE COMPLEXITY FOR 10% PERFORMANCE LOSS, $K = 8$ AND $M = 5$.

	FNN-DDPG	GNN-DDPG	GNN-DDPG +PE/PINN	GNN-DDPG +FNN	PE/PINN -DDPG	GNN-DDPG+PE/PINN with vanilla BN
Sample complexity	10000	800	800	7200	4000	1600
Compression ratio	12.5	1.0	1.0	9.0	5.0	2.0
Signaling overhead (GB)	3.6	0.3	0.3	2.6	1.4	0.5
Compression ratio	12.0	1.0	1.0	8.7	4.7	1.7

sharing for the GNNs used in the embedding manner and the end-to-end manner, designed the output layers for actor and critic networks when GNN is used in the embedding manner, and introduced a batch normalization method for permutable samples. We compared the DDPG algorithms where the actor and critic networks are GNNs and PE/PINNs, respectively. From simulations, we obtained the following observations for the considered problem. (1) Graph DDPG algorithm exploiting both kinds of relational priors achieves the same learning performance as the DDPG algorithm using the PE/PINNs to exploit only the PE/PI properties, but with much lower sample complexity and time complexity. (2) Graph DDPG algorithm converges much faster and needs much lower time complexity, space complexity, and signaling overhead for training than the DDPG with FNNs to achieve the same learning performance, especially for more users. (3) To exploit the PE/PI properties, batch normalization should be carefully designed, otherwise the sample complexity and time complexity will increase. (4) With appropriately designed output layer, the GNN used in the embedding manner performs very close to the GNN used in the end-to-end manner, in terms of both the learning performance and the training complexity.

APPENDIX A: PROOF OF PROPOSITION 1

Denote n_a as the number of vertexes of the a th type, where $a = 1, \dots, |\mathcal{A}|$ and \mathcal{A} is the set of vertex types. The index of all vertexes can be expressed as,

$$\left\{ \underbrace{1, \dots, n_1}_{\text{the first type}}, \underbrace{n_1 + 1, \dots, n_1 + n_2}_{\text{the second type}}, \dots, \sum_{a=1}^{|\mathcal{A}|} n_a \right\}. \quad (\text{A.1})$$

The index of all vertexes of the a_1 th type can be expressed as $\{\sum_{i=1}^{a_1-1} n_i + 1, \dots, \sum_{i=1}^{a_1} n_i\}$.

When we permute the vertexes of the a_1 th type, the index of all vertexes of this type can be expressed as $\tilde{\mathcal{N}}_{a_1} = \{\pi(n_{a_1+1} + 1), \dots, \pi(\sum_{i=1}^{a_1} n_i)\}$, where $\pi(\cdot)$ stands for the permutation operation on the index.

Recall that $\mathbf{d}_{t,m,a}^{(l)}$ and $\mathbf{d}_{t,m}^{(l)}$ are respectively the aggregation output and hidden output of the m th vertex in the l th layer at time step t , and L is the number of layers of the GNN. We use $\tilde{\mathbf{d}}_{t,m,a}^{(l)}$ and $\tilde{\mathbf{d}}_{t,m}^{(l)}$ to denote the aggregation output and hidden output of the m th vertex in the l th layer at time step t when we permute the vertexes of the a_1 th type.

Denote \mathcal{M} as the set of indices of all vertexes that are not permuted. We aim to prove that

$$\tilde{\mathbf{d}}_{t,m}^{(L)} = \mathbf{d}_{t,m}^{(L)}, \quad \forall m \in \mathcal{M}, \quad (\text{A.2a})$$

$$\tilde{\mathbf{d}}_{t,\pi(m)}^{(L)} = \mathbf{d}_{t,m}^{(L)}, \quad \forall m \in \mathcal{N}_{a_1}, \quad (\text{A.2b})$$

where (A.2a) indicates that the GNN satisfies (b) in Property 1, and (A.2b) indicates that the GNN satisfies (a) in Property 1.

If we can prove that

$$\tilde{\mathbf{d}}_{t,m}^{(l)} = \mathbf{d}_{t,m}^{(l)}, \quad \forall m \in \mathcal{M}, \quad (\text{A.3a})$$

$$\tilde{\mathbf{d}}_{t,\pi(m)}^{(l)} = \mathbf{d}_{t,m}^{(l)}, \quad \forall m \in \mathcal{N}_{a_1}, \quad (\text{A.3b})$$

are true for $\forall l$, then (A.2) holds when $l = L$. In the sequel, we use *Mathematical Induction* method to prove (A.3).

When $l = 0$, i.e., in the input layer, $\mathbf{d}_{t,m}^{(0)}$ is the feature of the vertexes. Because we do not permute the vertexes in \mathcal{M} , (A.3a) is true. The features of the vertexes in \mathcal{N}_{a_1} are permuted in the same way as the permuted vertexes in \mathcal{N}_{a_1} , hence (A.3b) is true.

In what follows, we prove that (A.3) is true when $l = l_0 + 1$ if (A.3) is true when $l = l_0$.

(i) *Prove that (A.3a) is true when $l = l_0 + 1$ if (A.3a) is true when $l = l_0$.*

According to (9) and (10), if we do not permute the vertexes of the a_1 th type, the hidden output of the m_0 th vertex in the $(l_0 + 1)$ th layer can be obtained as,

$$\mathbf{d}_{t,m_0,a}^{(l_0+1)} = \text{PL}_{n \in \mathcal{N}_{t,a}(m_0)}(q_{m_0,n}(\mathbf{d}_{t,n}^{(l_0)}, \mathbf{e}_{t,m_0}^n, \phi_{m_0,n}^{(l_0+1)})), \quad (\text{A.4a})$$

$$\mathbf{d}_{t,m_0}^{(l_0+1)} = \text{CB}_{m_0}(\mathbf{d}_{t,m_0}^{(l_0)}, \{\mathbf{d}_{t,m_0,a}^{(l_0+1)}, a \in \mathcal{A}\}, \theta_{m_0}^{(l_0+1)}), \quad m_0 \in \mathcal{M}. \quad (\text{A.4b})$$

(A.4b) represents a mapping from $\mathbf{d}_{t,m_0}^{(l_0)}$ and $\{\mathbf{d}_{t,m_0,a}^{(l_0+1)}, a \in \mathcal{A}\}$ into $\mathbf{d}_{t,m_0}^{(l_0+1)}$. If $\mathbf{d}_{t,m_0}^{(l_0)}$ and $\{\mathbf{d}_{t,m_0,a}^{(l_0+1)}, a \in \mathcal{A}\}$ remain unchanged when we permute the vertexes of the a_1 th type, then $\mathbf{d}_{t,m_0}^{(l_0+1)}$ is unchanged when permuting the vertexes of the a_1 th type.

The assumption that (A.3a) is true when $l = l_0$ and $m_0 \in \mathcal{M}$ indicates that $\mathbf{d}_{t,m_0}^{(l_0)}$ remains unchanged when we permute the vertexes of the a_1 th type. In the following steps of (a) and (b), we prove that $\{\mathbf{d}_{t,m_0,a}^{(l_0+1)}, a \in \mathcal{A}\}$ is unchanged when we permute the vertexes with the a_1 th type.

(a) We first prove that $\mathbf{d}_{t,m_0,a}^{(l_0+1)}$ remains unchanged for $\forall a \neq a_1$ when permuting the vertexes of the a_1 th type. Since we only permute the vertexes of the a_1 th type, the vertexes in $\{\mathcal{N}_{t,a}(m_0), a \neq a_1\}$ are not permuted and hence belong to \mathcal{M} . Thereby, both $\mathbf{d}_{t,n}^{(l_0)}$ and \mathbf{e}_{t,m_0}^n remain unchanged

for $n \in \{\mathcal{N}_{t,a}(m_0), a \neq a_1\}$, then from (A.4a) we know that $\mathbf{d}'_{t,m_0,a}^{(l_0+1)}$ remains unchanged for $\forall a \neq a_1$.

(b) We then prove that $\mathbf{d}'_{t,m_0,a}^{(l_0+1)}$ remains unchanged for $a = a_1$ when we permute the vertexes of the a_1 th type. Since the n th vertex and $\pi(n)$ th vertex are with the same type for $\forall n \in \mathcal{N}_{t,a_1}(m_0)$, the condition that the processor is identical when the vertexes with the same type aggregate the vertexes with the same type can be expressed as

$$q_{m_0,n}(\cdot, \cdot, \phi_{m_0,n}^{(l_0+1)}) = q_{m_0,\pi(n)}(\cdot, \cdot, \phi_{m_0,\pi(n)}^{(l_0+1)}), \quad \forall n \in \mathcal{N}_{t,a_1}(m_0). \quad (\text{A.5})$$

Recalling that $\mathcal{N}_{t,a_1}(m_0)$ is the set of vertexes of the a_1 th type neighboring to the m_0 th vertex at time step t and \mathcal{N}_{a_1} is the set of all the vertexes of the a_1 th type, it is not hard to show that $\mathcal{N}_{t,a_1}(m_0) \subseteq \mathcal{N}_{a_1}$. Then, the assumption that (A.3b) is true when $l = l_0$ can be expressed as

$$\tilde{\mathbf{d}}_{t,\sigma(n)}^{(l_0)} = \mathbf{d}_{t,n}^{(l_0)}, \quad \forall n \in \mathcal{N}_{t,a_1}(m_0). \quad (\text{A.6})$$

According to (A.5) and (A.6), and further considering that when we permute a vertex, the sets of its neighboring vertexes and the edges linked with it are permuted accordingly, we have

$$q_{m_0,n}(\mathbf{d}_{t,n}^{(l_0)}, \mathbf{e}_{t,m_0}^n, \phi_{m_0,n}^{(l_0+1)}) = q_{m_0,\pi(n)}(\tilde{\mathbf{d}}_{t,\pi(n)}^{(l_0)}, \mathbf{e}_{t,m_0}^{\pi(n)}, \phi_{m_0,\pi(n)}^{(l_0+1)}), \quad \forall n \in \mathcal{N}_{t,a_1}(m_0). \quad (\text{A.7})$$

According to (A.7), and further considering that the pooling function satisfies the commutative law, we can obtain

$$\text{PL}_{n \in \mathcal{N}_{t,a_1}(m_0)}(q_{m_0,n}(\mathbf{d}_{t,n}^{(l_0)}, \mathbf{e}_{t,m_0}^n, \phi_{m_0,n}^{(l_0+1)})) = \text{PL}_{n \in \tilde{\mathcal{N}}_{t,a_1}(m_0)}(q_{m_0,n}(\mathbf{d}_{t,n}^{(l_0)}, \mathbf{e}_{t,m_0}^n, \phi_{m_0,n}^{(l_0+1)})), \quad (\text{A.8})$$

where $\tilde{\mathcal{N}}_{t,a_1}(m_0)$ is the set of vertexes of the a_1 th type neighboring to the m_0 th vertex at time step t when we permute the vertexes with the a_1 th type, the left and right hand side of (A.8) respectively represent $\mathbf{d}'_{t,m_0,a_1}^{(l_0+1)}$ before and after permutation. (A.8) indicates that $\mathbf{d}'_{t,m_0,a_1}^{(l_0+1)}$ remains unchanged when we permute the vertexes with the a_1 th type.

From (A.4b) we know that $\mathbf{d}'_{t,m_0}^{(l_0+1)}$ remains unchanged, i.e., (A.3a) is true for the m_0 th vertex when $l = l_0 + 1$. Since the m_0 th vertex is arbitrarily chosen from \mathcal{M} , the proof holds for all the vertexes in \mathcal{M} . This completes the proof that (A.3a) is true when $l = l_0 + 1$.

(ii) *Prove that (A.3b) is true when $l = l_0 + 1$ if (A.3b) is true when $l = l_0$.*

The same as the proof in (i), we can prove that $\{\mathbf{d}'_{t,m_1,a}^{(l_0+1)}, a \in \mathcal{A}\}$ remains unchanged for $m_1 \in \mathcal{N}_{a_1}$ when we permute the vertexes of the a_1 th type, i.e.,

$$\mathbf{d}'_{t,m_1,a}^{(l_0+1)} = \tilde{\mathbf{d}}_{t,\pi(m_1),a}^{(l_0+1)}, \quad \forall a \in \mathcal{A}, \quad m_1 \in \mathcal{N}_{a_1}. \quad (\text{A.9})$$

The assumption that (A.3b) is true when $l = l_0$ and $m_1 \in \mathcal{N}_{a_1}$ can be expressed as

$$\mathbf{d}_{t,m_1}^{(l_0)} = \tilde{\mathbf{d}}_{t,\pi(m_1)}^{(l_0)}. \quad (\text{A.10})$$

If the pooling function and combiner are identical for the vertexes with the same type, the m_1 th vertex and $\pi(m_1)$ th vertexes will employ the same combiner, i.e.,

$$\text{CB}_{m_1}(\cdot, \cdot, \boldsymbol{\theta}_{m_1}^{(l_0+1)}) = \text{CB}_{\pi(m_1)}(\cdot, \cdot, \boldsymbol{\theta}_{\pi(m_1)}^{(l_0+1)}). \quad (\text{A.11})$$

By submitting (A.9), (A.10) and (A.11) into (A.4b), we can obtain

$$\begin{aligned} \mathbf{d}_{t,m_1}^{(l_0+1)} &= \text{CB}_{m_1}(\mathbf{d}_{t,m_1}^{(l_0)}, \{\mathbf{d}'_{t,m_1,a}{}^{(l_0+1)}, a \in \mathcal{A}\}, \boldsymbol{\theta}_{m_1}^{(l_0+1)}) \stackrel{(\text{A.9})}{=} \text{CB}_{m_1}(\mathbf{d}_{t,m_1}^{(l_0)}, \{\tilde{\mathbf{d}}'_{t,\pi(m_1),a}{}^{(l_0+1)}, a \in \mathcal{A}\}, \boldsymbol{\theta}_{m_1}^{(l_0+1)}) \\ &\stackrel{(\text{A.10})}{=} \text{CB}_{m_1}(\tilde{\mathbf{d}}_{t,\pi(m_1)}^{(l_0)}, \{\tilde{\mathbf{d}}'_{t,\pi(m_1),a}{}^{(l_0+1)}, a \in \mathcal{A}\}, \boldsymbol{\theta}_{m_1}^{(l_0+1)}) \stackrel{(\text{A.11})}{=} \text{CB}_{\pi(m_1)}(\tilde{\mathbf{d}}_{t,\pi(m_1)}^{(l_0)}, \{\tilde{\mathbf{d}}'_{t,\pi(m_1),a}{}^{(l_0+1)}, a \in \mathcal{A}\}, \boldsymbol{\theta}_{\pi(m_1)}^{(l_0+1)}) \\ &= \tilde{\mathbf{d}}_{t,\pi(m_1)}^{(l_0+1)}, \end{aligned}$$

i.e., (A.3b) is true for the m_1 th vertex when $l = l_0 + 1$. Since the m_1 th vertex is arbitrarily chosen from \mathcal{N}_{a_1} , the proof holds for all the vertexes in \mathcal{N}_{a_1} . This completes the proof that (A.3a) is true when $l = l_0 + 1$.

From the proof in (i) and (ii), we know that (A.3) is true for $\forall l$, hence (A.2) is true where $l = L$. This completes the proof for Proposition 1.

REFERENCES

- [1] N. Luong, D. Hoang, S. Gong, D. Niyato, P. Wang, Y. Liang, and D. Kim, "Applications of deep reinforcement learning in communications and networking: A survey," *IEEE Commun. Surveys Tuts.*, vol. 21, no. 4, pp. 3133–3174, Fourth quarter 2019.
- [2] Z. Zhang, Y. Yang, M. Hua, C. Li, Y. Huang, and L. Yang, "Proactive caching for vehicular multi-view 3D video streaming via deep reinforcement learning," *IEEE Trans. Wireless Commun.*, vol. 18, no. 5, pp. 2693–2706, May 2019.
- [3] J. Zhang, Y. Huang, J. Wang, and X. You, "Intelligent beam training for millimeter-wave communications via deep reinforcement learning," in *Proc. IEEE GLOBECOM*, 2019.
- [4] D. Liu, J. Zhao, and C. Yang, "Energy-saving predictive video streaming with deep reinforcement learning," in *Proc. IEEE GLOBECOM*, 2019.
- [5] A. Khan and R. Adve, "Centralized and distributed deep reinforcement learning methods for downlink sum-rate optimization," *IEEE Trans. Wireless Commun.*, vol. 19, no. 12, pp. 8410–8426, 2020.
- [6] K. Feng, Q. Wang, X. Li, and C. Wen, "Deep reinforcement learning based intelligent reflecting surface optimization for MISO communication systems," *IEEE Wireless Commun. Let.*, vol. 9, no. 5, pp. 745–749, May. 2020.
- [7] A. Kasgari, W. Saad, M. Mozaffari, and V. Poor, "Experienced deep reinforcement learning with generative adversarial networks (GANs) for model-free ultra reliable low latency communications," *IEEE Trans. Wireless Commun.*, vol. 69, no. 2, pp. 884–899, 2021.
- [8] M. Alsenwi, N. Tran, M. Bennis, S. Pandey, A. Bairagi, and C. Hong, "Intelligent resource slicing for eMBB and URLLC coexistence in 5G and beyond: A deep reinforcement learning based approach," *IEEE Trans. Wireless Commun.*, vol. 20, no. 7, pp. 4585–4600, 2021.
- [9] S. Wang, T. Lv, W. Ni, N. Beaulieu, and Y. Guo, "Joint resource management for MC-NOMA: A deep reinforcement learning approach," *IEEE Trans. Wireless Commun.*, vol. 20, no. 9, pp. 5672–5688, 2021.

- [10] N. Bui, M. Cesana, S. A. Hosseini, Q. Liao, I. Malanchini, and J. Widmer, "A survey of anticipatory mobile networking: Context-based classification, prediction methodologies, and optimization techniques," *IEEE Commun. Surv. Tutorials*, vol. 19, no. 3, pp. 1790–1821, Apr. 2017.
- [11] U. Challita, L. Dong, and W. Saad, "Proactive resource management for LTE in unlicensed spectrum: A deep learning perspective," *IEEE Trans. Wireless Commun.*, vol. 17, no. 7, pp. 4674–4689, Jul. 2018.
- [12] A. Azari, P. Papapetrou, S. Denic, and G. Peters, "User traffic prediction for proactive resource management: Learning-powered approaches," *IEEE GLOBECOM*, 2019.
- [13] F. Liu, W. Yuan, C. Masouros, and J. Yuan, "Radar-assisted predictive beamforming for vehicular links: Communication served by sensing," *IEEE Trans. Wireless Commun.*, vol. 19, no. 11, pp. 7704–7719, Nov. 2020.
- [14] C. Lee, H. Cho, S. Song, and J. Chung, "Prediction-based conditional handover for 5G mm-Wave networks: A deep-learning approach," *IEEE Veh. Technol. Mag.*, vol. 15, no. 1, pp. 54–62, 2020.
- [15] D. Tsilimantos, A. Nogales-Gómez, and S. Valentin, "Anticipatory radio resource management for mobile video streaming with linear programming," in *Proc. IEEE ICC*, 2016.
- [16] N. Bui and J. Widmer, "Data-driven evaluation of anticipatory networking in LTE networks," *IEEE Trans. on Mobile Comput.*, vol. 17, no. 10, pp. 2252–2265, Oct. 2018.
- [17] R. Atawia, H. S. Hassanein, H. Abou-Zeid, and A. Noureldin, "Robust content delivery and uncertainty tracking in predictive wireless networks," *IEEE Trans. Wireless Commun.*, vol. 16, no. 4, pp. 2327–2339, Apr. 2017.
- [18] Z. Lu and G. Veciana, "Optimizing stored video delivery for wireless networks: The value of knowing the future," *IEEE Trans. Multimedia*, vol. 21, no. 1, pp. 197–210, May 2019.
- [19] C. She and C. Yang, "Energy efficient resource allocation for hybrid services with future channel gains," *IEEE Trans. Green Commun. and Netw.*, vol. 4, no. 1, pp. 165–179, Mar. 2020.
- [20] Cisco, "Cisco annual internet report, 2018–2023 white paper," 2020. [Online]. Available: <https://www.cisco.com/c/en/us/solutions/collateral/executive-perspectives/annual-internet-report/white-paper-c11-741490.pdf>
- [21] V. Zambaldi, D. Raposo, A. Santoro, V. Bapst, Y. Li, I. Babuschkin, K. Tuyls, D. Reichert, T. Lillicrap, E. Lockhart *et al.*, "Relational deep reinforcement learning," *arXiv preprint*, 2018. [Online]. Available: <https://arxiv.org/pdf/1806.01830.pdf>
- [22] M. Zaheer, S. Kottur, S. Ravanbakhsh, B. Póczos, R. Salakhutdinov, and A. Smola, "Deep sets," *Advances in Neural Information Processing Systems*, 2017.
- [23] C. Sun, J. Wu, and C. Yang, "Improving learning efficiency for wireless resource allocation with symmetric prior," *IEEE Wireless Commun.*, accepted, 2021.
- [24] M. Eisen and A. Ribeiro, "Optimal wireless resource allocation with random edge graph neural networks," *IEEE Trans. Signal Process.*, vol. 68, no. 10, pp. 2977–2991, 2020.
- [25] Y. Shen, Y. Shi, J. Zhang, and K. B. Letaief, "Graph neural networks for scalable radio resource management: Architecture design and theoretical analysis," *IEEE J. Sel. Areas Commun.*, vol. 39, no. 1, pp. 101–115, 2020.
- [26] M. Lee, G. Yu, and G. Y. Li, "Graph embedding-based wireless link scheduling with few training samples," *IEEE Trans. Wireless Commun.*, vol. 20, no. 4, pp. 2282–2294, 2020.
- [27] J. Guo and C. Yang, "Learning power allocation for multi-cell-multi-user systems with heterogeneous graph neural network," *IEEE Trans. Wireless Commun.*, vol. 21, no. 2, pp. 884–897, 2022.
- [28] K. Nakashima, S. Kamiya, K. Ohtsu, K. Yamamoto, T. Nishio, and M. Morikura, "Deep reinforcement learning-based channel allocation for wireless LANs with graph convolutional networks," *IEEE Access*, vol. 8, pp. 31 823–31 834, 2020.
- [29] O. Orhan, V. N. Swamy, T. Tetzlaff, M. Nassar, H. Nikopour, and S. Talwar, "Connection management xAPP for O-RAN RIC: A graph neural network and reinforcement learning approach," in *Proc. IEEE ICMLA*, 2021.

- [30] P. Sun, J. Lan, J. Li, Z. Guo, and Y. Hu, "Combining deep reinforcement learning with graph neural networks for optimal VNF placement," *IEEE Commun. Lett.*, vol. 25, no. 1, pp. 176–180, Jan. 2021.
- [31] Z. Wu, S. Pan, F. Chen, G. Long, C. Zhang, and P. Yu, "A comprehensive survey on graph neural networks," *IEEE Trans. Neural Netw. Learn. Syst.*, vol. 32, no. 1, pp. 4–24, 2021.
- [32] S. Ioffe and C. Szegedy, "Batch normalization: Accelerating deep network training by reducing internal covariate shift," *Proc.ICML*, 2015.
- [33] T. Lillicrap, J. Hunt, A. Pritzel, N. Heess, T. Erez, Y. Tassa, D. Silver, and D. Wierstra, "Continuous control with deep reinforcement learning," in *Proc. ICLR*, 2015.
- [34] G. Dalal, K. Dvijotham, M. Vecerik, T. Hester, C. Paduraru, and Y. Tassa, "Safe exploration in continuous action spaces," *arXiv preprint*, 2018. [Online]. Available: <http://arxiv.org/abs/1801.08757>
- [35] S. Ravanbakhsh, J. Schneider, and B. Póczos, "Equivariance through parameter-sharing," in *Proc. JMCR ICML*, 2017.
- [36] Y. Carl, X. Yuxin, Z. Yu, S. Yizhou, and H. Jiawei, "Heterogeneous network representation learning: A unified framework with survey and benchmark," *IEEE Trans. Knowl. Data En.*, Early Access, 2020.
- [37] *ETSI TR 138 901 V14.3.0: 5G; Study on channel model for frequencies from 0.5 to 100 GHz*, 3GPP Std. 3GPP TR 38.901 version 14.3.0 release 14, 2018.
- [38] "Youtube. recommended upload encoding setting." Accessed: Sep. 26. 2021. [Online]. Available: <https://support.google.com/youtube/answer/1722171>
- [39] N. Aschenbruck, R. Ernst, E. Gerhards-Padilla, and M. Schwamborn, "Bonnmotion: A mobility scenario generation and analysis tool," 2010.
- [40] D. P. Kingma and J. Ba, "Adam: A method for stochastic optimization," in *Proc. ICLR*, 2014.